

ARTICLE OPEN



Fully implantable and battery-free wireless optoelectronic system for modifiable cancer therapy and real-time monitoring

Kiho Kim^{1,13}, In Sik Min^{1,13}, Tae Hee Kim^{2,3,13}, Do Hyeon Kim⁴, Seungwon Hwang⁵, Kyowon Kang¹, Kyubeen Kim¹, Sangun Park^{2,6}, Jongmin Lee⁷, Young Uk Cho¹, Jung Woo Lee⁸, Woon-Hong Yeo^{9,10,11}, Young Min Song⁴✉, Youngmee Jung¹²✉ and Ki Jun Yu^{1,12}✉

Photodynamic therapy (PDT) is attracting attention as a next-generation cancer treatment that can selectively destroy malignant tissues, exhibit fewer side effects, and lack pain during treatments. Implantable PDT systems have recently been developed to resolve the issues of bulky and expensive conventional PDT systems and to implement continuous and repetitive treatment. Existing implantable PDT systems, however, are not able to perform multiple functions simultaneously, such as modulating light intensity, measuring, and transmitting tumor-related data, resulting in the complexity of cancer treatment. Here, we introduce a flexible and fully implantable wireless optoelectronic system capable of continuous and effective cancer treatment by fusing PDT and hyperthermia and enabling tumor size monitoring in real-time. This system exploits micro inorganic light-emitting diodes (μ -LED) that emit light with a wavelength of 624 nm, designed not to affect surrounding normal tissues by utilizing a fully programmable light intensity of μ -LED and precisely monitoring the tumor size by Si phototransistor during a long-term implantation (2–3 weeks). The superiority of simultaneous cancer treatment and tumor size monitoring capabilities of our system operated by wireless power and data transmissions with a cell phone was confirmed through in vitro experiments, ray-tracing simulation results, and a tumor xenograft mouse model in vivo. This all-in-one single system for cancer treatment offers opportunities to not only enable effective treatment of tumors located deep in the tissue but also enable precise and continuous monitoring of tumor size in real-time.

npj Flexible Electronics (2023)7:41 | <https://doi.org/10.1038/s41528-023-00276-x>

INTRODUCTION

The number of deaths due to cancer worldwide is estimated at 10 million in 2020 and has continued to increase for decades¹. Conventional representative cancer treatments such as surgical operation, radiation therapy, and chemotherapy are effective, but there are side effects and aftereffect problems^{2,3}. In the case of tumor resection, a malignant tissue can be effectively removed, but additional resection of surrounding normal tissues may result in organ function loss or, in serious cases, may threaten the patient's life^{4–6}. Radiation therapy is widely used for the treatment of local tumors, but it can be exposed to a variety of side effects, including vomiting, hair loss, and skin damage^{7,8}. Chemotherapy is effective in treating cancer that has spread throughout the body, but it puts a lot of strain on the patient's body because it causes various side effects such as cardiac dysfunction, weakened immune system, or even cognitive impairment^{9–11}.

Photodynamic therapy (PDT) is receiving a lot of attention as a treatment option for curing cancer that can resolve the aforementioned issues with the existing cancer treatments due

to its high selectivity for cancer cells to destroy and fewer side effects¹². PDT selectively destructs tumor tissues by injecting a photoreactive drug, called a photosensitizer, inducing a photodynamic response only in tumor cells when light with an absorbable wavelength is illuminated on the tissue¹³. However, conventional PDT systems using a laser equipment with an endoscope or optical fibers have some critical limitations. First, endoscopes and optical fibers can deliver light only to the exposed epithelial tissue with a shallow penetration depth less than 1 cm¹⁴, which greatly limits the applicable range of PDT. In addition, the laser with high intensity and coherency induces a rapid photodynamic reaction within a short time, thereby resulting in reduced the therapeutic effect¹⁵. Another problem of the existing laser-based PDT system is that the accessibility of treatment and its portability are poor due to the bulkiness of the laser equipment and its relatively high price¹⁶. To overcome these limitations, wireless implantable PDT systems have been actively developed recently^{14,17–19}. They provide improved accessibility and therapeutic effect because implantable PDT systems with a wireless operation in the human body are not limited to hospitals

¹Functional Bio-integrated Electronics and Energy Management Lab, School of Electrical and Electronic Engineering, Yonsei University, 50 Yonsei-ro, Seodaemun-gu, Seoul 03722, Republic of Korea. ²Center for Biomaterials, Biomedical Research Institute, Korea Institute of Science and Technology (KIST), Seoul 02792, Republic of Korea. ³Department of Fusion Research and Collaboration, Biomedical Research Institute, Seoul National University Hospital, Seoul 03080, Republic of Korea. ⁴School of Electrical Engineering and Computer Science (EECS), Gwangju Institute of Science and Technology (GIST), Gwangju 61005, Republic of Korea. ⁵PA1, Foundry Business, Samsung Electronics, 1 Samsungjeonja-ro, Hwaseong-si, Gyeonggi-do, Republic of Korea. ⁶R&D Center DNA Lab, Pharmaresearch, Seongnam 13486, Republic of Korea. ⁷KU-KIST Graduate School of Converging Science and Technology, Korea University, Seoul 136-705, Republic of Korea. ⁸School of Materials Science and Engineering, Energy Materials for Soft Electronics Laboratory, Pusan National University, Busan 46241, Republic of Korea. ⁹IEN Center for Human-Centric Interfaces and Engineering and George W. Woodruff School of Mechanical Engineering, Georgia Institute of Technology, Atlanta, GA 30332, USA. ¹⁰Wallace H. Coulter Department of Biomedical Engineering, Georgia Institute of Technology and Emory University School of Medicine, Atlanta, GA 30332, USA. ¹¹Institute for Robotics and Intelligent Machines, Parker H. Petit Institute for Bioengineering and Biosciences, Institute for Materials, Neural Engineering Center, Georgia Institute of Technology, Atlanta, GA 30332, USA. ¹²School of Electrical and Electronic Engineering, YU-Korea Institute of Science and Technology (KIST) Institute, Yonsei University, 50, Yonsei-ro, Seodaemun-gu, Seoul 03722, Republic of Korea. ¹³These authors contributed equally: Kiho Kim, In Sik Min, Tae Hee Kim. ✉email: ymsong@gist.ac.kr; winnie97@kist.re.kr; kijunyu@yonsei.ac.kr

and can be operated anytime, anywhere and can also deliver light to deep tumors, greatly expanding the usable range of PDT. However, these systems still have drawbacks in that they employ non-fully implantable devices that can cause infections at the insertion site, or rigid form factors that can damage soft biological tissues¹⁴. In addition, even systems that use the fully implantable device of flexible form factors still lack functionality such as light intensity modulation¹⁷ or tumor-related measurements¹⁹ due to passive electronics. Furthermore, because of the low level of encapsulations, the operation stability of the devices in vivo environments has not been secured for more than a few weeks¹⁸. Along with PDT, hyperthermia, a cancer treatment that involves exposing cancerous tissue to high temperatures in order to either kill the cancer cells directly or make them more sensitive to other forms of therapy, is also one of the most promising approaches for cancer treatment^{20,21}. However, while conventional hyperthermia is sometimes effective in treating cancer cells, but it often kills normal tissues. Researchers have been working on developing more localized hyperthermia techniques that can produce a temperature increase that is confined to the tumor. This can be achieved through techniques such as focused ultrasound²², which uses high-frequency sound waves to heat the tumor directly, or nanoparticle-mediated hyperthermia²³, which uses nanoparticles to deliver heat to the tumor. These methods aim to minimize the exposure of healthy tissue to high temperatures, reducing the risk of side effects and increasing the effectiveness of the therapy.

In continuous and repeatable cancer treatment modalities including PDT and hyperthermia, monitoring cancer progression concurrently with treatment is important to evaluate and improve treatment effectiveness. This is typically done through regular imaging studies^{24,25}, such as computed tomography (CT) scans, or bioluminescence. These tests help to determine the size and spread of cancer and can help guide decisions about treatment options and adjustments. However, CT and bioluminescence are unable to achieve a good level of temporal resolution over long monitoring periods. This is because CT imaging requires the use of radiation and contrast dyes, which can have toxicity limitations, and these imaging methods also tend to be resource-intensive and costly. As a result, it can be difficult to use these techniques to image large groups of patients or to take frequent measurements over time. To address these issues, a study on continuous monitoring of tumor volume using a flexible strain sensor has recently been conducted, but it has limitations in that it cannot treat cancer and only diagnoses the progress of cancer²⁶. Also, recently developed functional photosensitizing agents have demonstrated the potential for real-time monitoring of therapeutic efficacy indicators associated with PDT through external imaging systems^{27–32}. However, a fully integrated system capable of simultaneously performing PDT and tumor monitoring within the body, without the need for separate imaging systems, has not been reported.

Here, we propose a flexible and fully implantable, battery-free, optoelectronic system that enables continuous and modifiable PDT with hyperthermia utilizing fully programmable light intensity, and tumor size monitoring system during long-term treatment. We designed the device to effectively transfer light from the inside of the tumor through the insertion of the μ -LED probe and to allow heat generated from the μ -LED to act solely as a factor for cancer treatment without affecting the surrounding normal tissues. Also, the phototransistor located at the back of the probe can measure the amount of light scattered through the tumor to obtain information about the change in tumor size. Biocompatible black PDMS was used to prevent the interference of μ -LED light transmitted through the encapsulation layer, enabling accurate tumor size monitoring. To wirelessly control the intensity of the μ -LED and record the measurements of the phototransistor, the Bluetooth Low Energy (BLE) communication system is embedded in the device and a customized smartphone

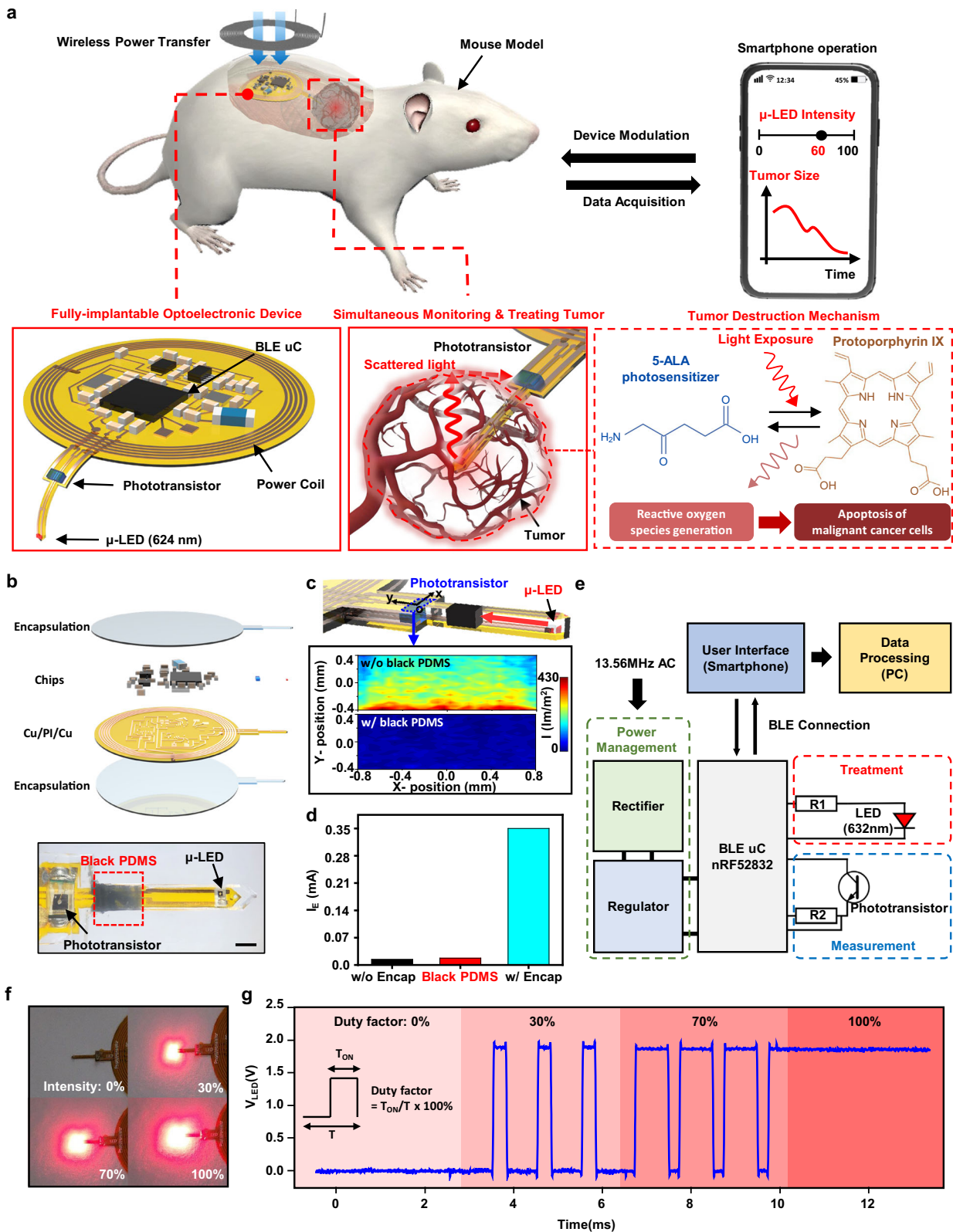
application was developed for data transmission and reception on the user side. To guarantee the long-term operation and biocompatibility of our system in vivo environments^{33–35}, a thin-multilayer encapsulation is applied. We confirm the cancer-curing efficacy and tumor growth monitoring performance of the system through in vitro, ex vivo experiment and ray-tracing simulation. Finally, we subcutaneously implanted fully implantable wireless PDT with hyperthermia and cancer monitoring system in nude mice to perform treatment and measurement for tumor transplanted into the dorsal flanks. The animal experiments showed the reliable cancer progress estimating and remarkable antitumor effects of the system.

RESULTS

Fully implantable wireless optoelectronic system for cancer treatment and monitoring

Figure 1a shows the overall working principle of an all-in-one system consisting of a light delivery system for cancer treatment, an optical measurement system for tumor size estimation, and a wireless communication system for device modulation and data acquisition. After injecting human colorectal cancer cells (HCT-15) subcutaneously into the dorsal flanks of a BALB/c nude mouse, the probe part of the device is inserted into the tumor, while the entire device is fully implanted subcutaneously on the dorsal side near the tumor. Once the photosensitizer 5-ALA is absorbed by the tumor cells and converted to Protoporphyrin IX (PpIX), an alternating current flowing coil delivers power to activate the Bluetooth system wirelessly. Then, the μ -LED is operated to perform PDT and hyperthermia for more effective cancer treatment for a long period of time (~3 weeks). The intensity of μ -LED can be modulated by the user, depending on the progression of cancer, using a smartphone and the custom-designed Android application. At the same time, since the degree of light from the μ -LED scattered inside the tumor is affected by the tumor's size, the cancer progression is monitored in real-time by a phototransistor outside the tumor (Supplementary Video 1).

The fully implantable wireless PDT with hyperthermia and cancer monitoring system is fabricated by mounting chips for wireless communication, including a phototransistor, a μ -LED, and a BLE system on a chip (SoC), and other operating chips on a thin flexible printed circuit board (FPCB) (Fig. 1b). A bilayer metal line is formed through via to increase the degree of circuit integration for device miniaturization. The thicknesses of the copper line and the PI substrate are 18 μ m and 25 μ m, respectively. The multi-stacked structure of Polydimethylsiloxane (PDMS)/SiO₂/polyene C is applied both on top and bottom of the device for encapsulation to provide long-term operation by preventing the penetration of biofluids when implanting the device into a mouse. The whole device can be used as a biocompatible material in the body without side effects caused by by-products (Supplementary Fig. S9). However, the multi-stacked encapsulant causes significant light noise from the μ -LED due to total internal reflection (TIR). This noise leads to minimal voltage changes for varying tumor sizes, which can interfere with accurate tumor size measurements (Supplementary Fig. S13). As a solution, we applied a biocompatible black PDMS, a mixture of PDMS and black food coloring, as a light-blocking layer between the μ -LED and the phototransistor. The black PDMS layer effectively blocks the light transmission resulting from TIR, as the black encapsulant absorbs the light before it reaches the phototransistor. The ray-tracing simulation results confirm that the black PDMS layer significantly reduces light noise into the phototransistor (Fig. 1c). The phototransistor's emitter current with three different encapsulants (w/o, w/ PDMS encapsulation, and w/ black PDMS encapsulation), measured when the μ -LED turned on in a dark room, demonstrates that the black encapsulant inhibits the light transmission resulting from



TIR, consistent with the simulation results (Fig. 1d). Detailed geometrical conditions and methods for the optical analysis appear in Methods and Supplementary Fig. S11.

The electronic circuit and wireless communication system consists of four main parts: a power management system for

wireless power receiving, a SoC for BLE communications, the μ -LED and the photo-detecting sensor for cancer therapy and monitoring, and the user interface for controlling light delivery and receiving data from the photo-detecting sensor (Fig. 1e). The 13.56 MHz AC power generated by external equipment is received

Fig. 1 Fully implantable wireless optoelectronic system for cancer treatment and monitoring. **a** Overall concept of cancer treatment and monitoring system including device schematic, principle of device operation that enables fully programmable μ -LED intensity control and real-time monitoring of tumor size, and chemical mechanism of PDT. **b** Exploded view of the device with PDMS/SiO₂/parlylene C encapsulation layers (top) and the photograph of the probe part containing black PDMS for blocking internally reflected light (bottom); Scale bar, 1 mm. **c** Ray-tracing simulation of the light flux into the phototransistor from the μ -LED with and without black PDMS. **d** Emitter current measurement of phototransistor when the μ -LED is on in a dark room with three different encapsulants (w/o, w/ PDMS encapsulation, and w/ black PDMS encapsulation). **e** Block diagram of electronic components for wireless operation including wireless power transfer, light delivery control, photocurrent measurement, and wireless communication with a smartphone. **f** Photograph of pulse width modulated μ -LEDs with intensity of 0%, 30%, 70%, and 100%. **g** Forward voltage of the μ -LED when duty factor is sequentially changed to 30%, 70%, and 100% from 0%.

by the planar coil of the device, which is connected to a full-bridge rectifier consisting of four Schottky diodes. Once the input AC voltage is rectified, a regulator chip (LTC3255) regulates the supply voltage level to 3.3 V. After the BLE SoC (nRF52832) is powered up by the power management system, it automatically executes programmed firmware for handling wireless communication and interacting with various peripheral modules, including timers and general-purpose input-output (GPIO) pins. The μ -LED is controlled by a GPIO pin, and the emitter voltage of the phototransistor is recorded by a successive approximation analog-to-digital converter (SAADC) module inside the SoC. The custom-designed smartphone application provides an intuitive user interface to control the light intensity of the μ -LED just by swiping a bar, and the real-time data measured from the phototransistor can be exported to other computing devices, such as personal computers or mobile phones, in an organized text file format for processing.

Light intensity is one of the most important factors in determining the therapeutic effect of PDT, and the degree and spatial range of photodynamic reactions can be adjusted according to the control of light intensity^{19,36}. Implantable optoelectronic devices with only passive components are hardly able to modulate their designed stimulation pattern. However, a system consisting of programmable active parts, such as microcontrollers, can freely and precisely control the intensity or temporal pattern of stimulation even after being inserted into the living body, according to wireless control inputs. This means that it can provide a flexible performing method suitable for the patient's current pathological state. In our device, the intensity of the μ -LED, with a maximum brightness of 0.49 lm and a power of 5 mW, is controlled by the pulse width modulation (PWM) method. This method determines the brightness of the μ -LED by adjusting the on/off time ratio in the continuous pulse wave generated from the GPIO pin. The frequency of the pulse waves is programmed to be set at 1 kHz, and the duty factor representing the on/off time ratio of each pulse wave can be precisely controlled from 0% to 100% by wireless input through a BLE connection with a smartphone (Fig. 1f, g).

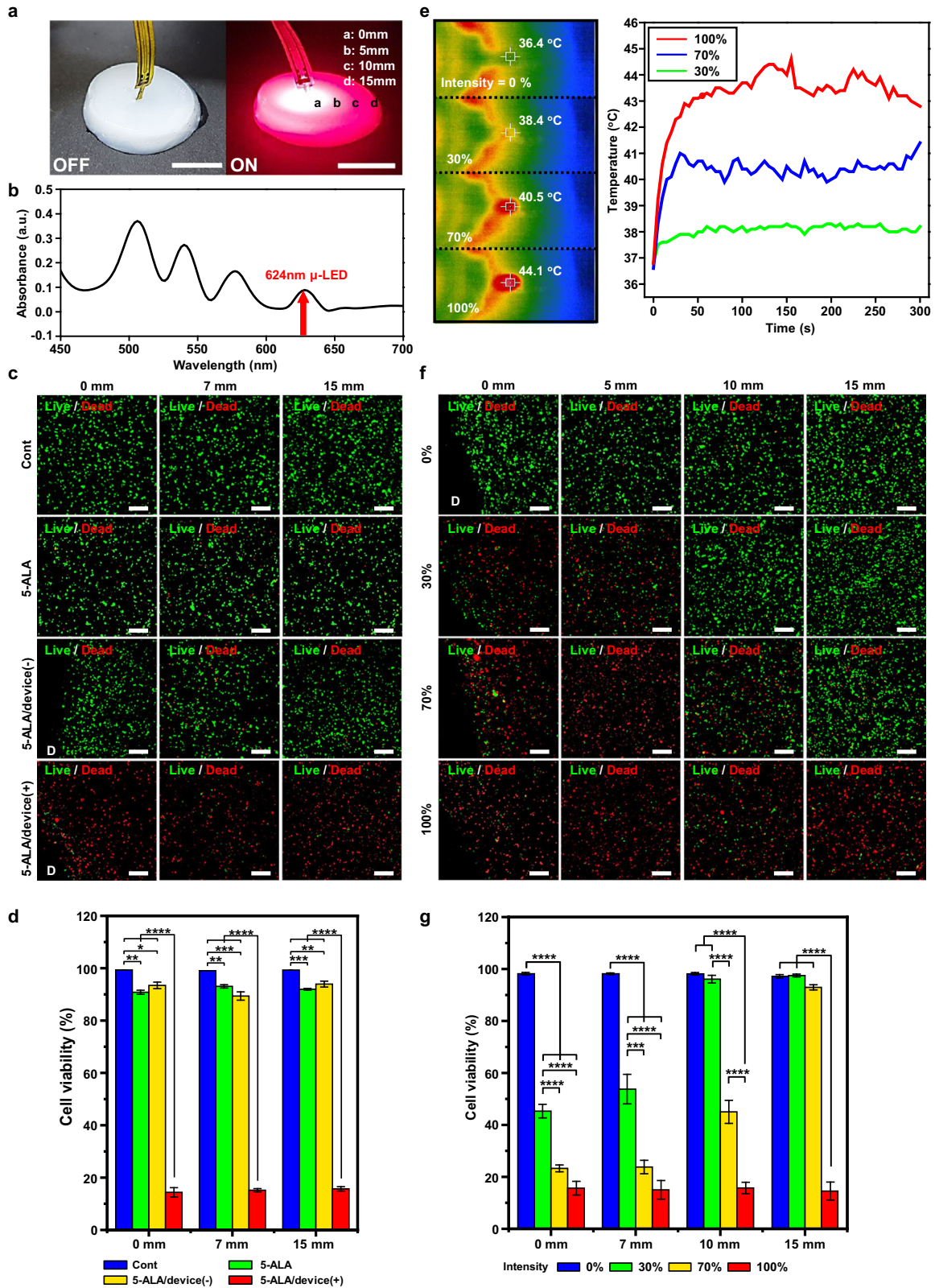
PDT efficacy of system in vitro

We established an HCT-15-based tumor-mimic tissue model to investigate the therapeutic effects of the device in vitro. The model simulated the tumor microenvironment using a hydrogel composed of collagen type I and fibrin, which are the main components that constitute the ECM of tumor tissue. The device was inserted into the center of the tumor-mimic tissue model fabricated in a cylindrical shape with a diameter of 3 cm and a depth of 5 mm, and the μ -LED of the device was turned on for 30 min to irradiate the tumor-mimic tissue with light (Fig. 2a). To determine the wavelength of the μ -LED to be used in our system, the absorption spectrum of PpIX was measured using an ultraviolet-visible-near-infrared spectrometer (Fig. 2b). PpIX exhibited absorption at various wavelengths, and we used an μ -LED with a wavelength of 624 nm to maximize the efficiency of light transmitted from the inside of the tumor to the outside when measuring the tumor volume.

In order to evaluate the efficacy of the PDT using the device, cell viability was analyzed according to the distance from the center of the tumor-mimic tissue in the following four treatment groups (Fig. 2c): (1) non-treatment group (Cont), (2) 5-ALA alone treatment group (5-ALA), (3) 5-ALA and device without μ -LED light treatment group (5-ALA/device (-)), (4) 5-ALA and device with μ -LED light treatment group (5-ALA/device (+)). In the 5-ALA/device (+) group, cell viability was 14.38%, 15.19%, and 15.69% at distances of 0, 7, and 15 mm from the center, respectively, which were 6.91-, 6.52-, and 6.33-fold lower than those of the control group, respectively (Fig. 2d). On the other hand, in the 5-ALA group and the 5-ALA/device (-) group, the cell viability according to the distance decreased significantly compared to the control group at all distances, but all of the values were higher than 85% as follows.; 5-ALA group: 90.83% (0 mm), 93.07% (7 mm), 91.95% (15 mm), and 5-ALA/device (-) group: 93.43% (0 mm), 89.38% (7 mm), 93.94% (15 mm). The low-level activation of PpIX, synthesized as 5-ALA is metabolized by daylight received during the experiment, is expected to be the reason for these results. The absorption peak of PpIX between 480 and 650 nm is contained in daylight, which is in the range of the visible spectrum between 380 and 780 nm. There was no significant difference in cell viabilities between the 5-ALA group and the 5-ALA/device (-) group at all distances, indicating that the device material hardly induces cell death.

As the device operates inside the body, the normal tissues surrounding it can be affected by the heat generated by the μ -LED. The temperature changing according to the μ -LED intensity at 36.5 °C was measured using a thermal imaging camera (Fig. 2e). In the case of 100% intensity, the temperature change of the μ -LED was 7 °C or higher. At 70% intensity, the temperature change was about 4 °C, and at 30% intensity, the temperature change was less than 1 °C. Since the intensity of light can be modulated at the user's discretion based on the size of the tumor, PDT can be effectively performed without affecting normal tissues using our system.

We also estimated the PDT efficacy for different light intensities by adjusting the light intensities using the device. For this, the tumor-mimicking tissue treated with 5-ALA was irradiated with μ -LED light at 0%, 30%, 70%, and 100% light intensity, respectively, and the cell viability was analyzed at various distances from the irradiation point (Fig. 2f). The cell viability at all distances was the lowest at 100% light intensity, followed by 70% and 30%, and the highest at 0% (Fig. 2g). In addition, when the light intensity was 0% and 100%, the cell viability was similar at all distances, approximately 98% and 15%, respectively. However, at 30% and 70% light intensity, the cell viability gradually increased as the distance increased. In particular, when the light intensity was 70%, the cell viability was not significantly different at both 0 and 5 mm distances compared to 100% light intensity. But at 10 and 15 mm distances, the cell viability increased by 2.86 and 6.39 times compared to 100%, respectively. These results suggest that the device can maximize PDT efficacy by effectively terminating cancer cells while minimizing damage to surrounding normal tissues by adjusting the light irradiation intensity according to the size of the tumor tissue.



Evaluation of tumor size monitoring system ex vivo and in vivo

A tumor xenograft mouse model using human tumor cell lines, which have been well established for decades, is the most commonly used tumor model for the study of human cancer in

mice due to its ease of generation³⁷. We utilized a human colorectal cancer cell-based xenograft mouse model, where HCT-15 cell suspension was subcutaneously injected into the dorsal flanks of BALB/c nude mice, to evaluate the efficacy of the cancer therapy and monitoring device in vivo (Fig. 3a). Two weeks after

Fig. 2 PDT efficacy of system in vitro. **a** μ -LED ON/OFF image of device inserted in human colorectal cancer cell (HCT-15)-based tumor-mimicking tissue model. Scale bar, 1 cm. **b** Absorption spectrum of protoporphyrin IX (PpIX), a metabolite of 5-ALA, between 450 and 700 nm. Red arrows indicate emission peak wavelengths of 624 nm. **c** Representative live/dead assay images according to the distance from the center in tumor-mimic tissue model treated with 5-ALA, 5-ALA and device without μ -LED light (5-ALA/device(-)), and 5-ALA and device with μ -LED light (5-ALA/device(+)). The control group (Cont) did not any treatment. Scale bar, 200 μ m. **d** Quantification of cell viability (%) in each treatment group according to the distance from the center of tumor-mimic tissue model. **e** Thermal images of μ -LED probe and temperature changes of μ -LED according to each intensity 0%, 30%, 70%, and 100%. **f** Representative live/dead assay images according to the distance from the center in tumor-mimic tissue model treated with μ -LED light of various intensities, and **(g)** quantification of the corresponding cell viability (%). Live cells are visualized as green and the dead cells as red. Data are expressed as the mean \pm SEM. * $p < 0.05$, ** $p < 0.01$, *** $p < 0.001$, or **** $p < 0.0001$. Scale bar, 200 μ m.

injection, the device was implanted subcutaneously on the dorsal side of mice whose tumors had reached 5–7 mm, and the μ -LED of the device was inserted into the center of the tumor. The probe part of the device was sutured to the fascia near the tumor to secure the μ -LED in place. Finally, a 13.56 MHz electromagnetic wave was wirelessly transmitted through a commercial external coil to operate the device, and the intensity of the μ -LED was adjusted. Data on the volume of the tumor were received in real-time using the developed smartphone application.

To analyze the dependence of light flux on tumor size, we conducted 3-dimensional ray-tracing simulations for three different tumor diameters ($D = 4, 8,$ and 11 mm) (Fig. 3b). We used optical coefficients of human colon tumors in the simulation to obtain accurate results³⁸. The light source ($\lambda = 630$ nm) was placed at the center of the tumor model. As shown in the ray-tracing scheme, the tumor strongly scatters light rays due to its high scattering coefficient (~ 120 cm⁻¹) (Supplementary Table 2). As the tumor size increases, the tumor gets closer to the phototransistor, which increases the amount of scattered light that can reach the phototransistor. This increases in light flux as the tumor volume increases, enabling precise tumor size monitoring. The light flux is barely attenuated with an increase in tumor volume due to the relatively lower absorption coefficient (~ 1 cm⁻¹) than the scattering coefficient (~ 120 cm⁻¹). This notable change in light intensity allows for precise sensing of tumor size owing to the inhibiting noise by black encapsulation (Supplementary Fig. S12). In contrast, the device without a black encapsulant limits simultaneous diagnostics due to a minimal change in the voltage (Supplementary Fig. S13). Moreover, we authenticated the proficiency of our system in measuring tumor size when our setup, inclusive of the tumor, is encompassed by PBS and normal tissue, by conducting ray tracing simulation (Supplementary Fig. S16).

The amount of emitter current is adjusted based on the size of the tumor, which is determined by changes in light transfer from the μ -LED inserted into the tumor to the external phototransistor. The size of the tumor is estimated by measuring the voltage value V_{PD} applied to the load resistor with an emitter follower circuit (Fig. 3d). To verify the tumor volume measuring performance of our system *ex vivo*, we used five HCT-15 tumors of different sizes: 57, 163, 199, 941, and 1671 mm³ (Fig. 3e). For each tumor, μ -LED probes from three different devices were inserted into three different points on the tumor surface, reaching the center of the tumors, and the emitter currents were measured. The size of the tumor can be estimated by proportionally increasing the emitter voltage value, which is consistent with the previous ray-tracing simulation results. However, the daily movement of the mouse could result in slight variations in the position of the μ -LED within the tumor, and if the μ -LED is not positioned at the center of the tumor, the measurement values can vary. Thus, phototransistor voltage (V_{PD}) values are measured as the μ -LED positioning changes from the center of the tumor, with respect to different tumor sizes (Supplementary Fig. S15). Ultimately, while there were minor changes in V_{PD} values depending on the position of the μ -LED within the tumor, the degree of light scattering inside the tumor was far more dominant depending on the size of the tumor, which allowed us to reliably distinguish tumor sizes.

Since BALB/c nude mice lack immunity to cancer, the size of the tumor naturally increases in the absence of any treatment. To verify the cancer growth monitoring performance of our system in an *in vivo* environment, we allowed tumors to grow naturally for 3 weeks after the device was implanted into mice ($n = 4$) and measured V_{PD} values indicating an emitter current of a phototransistor every week along with tumor volume, while the μ -LED was turned on at 50% brightness for 1 min (Fig. 3g). The results show the normalized V_{PD} values correlated with the normalized tumor size for each mouse (Fig. 3f). The mice with data covering two-week span represent instances where the tumor size grew excessively or the stability of the device's operation became challenging during *in vivo* experimentation, thereby necessitating an early termination of the experiment compared to the initial timeline. In the case of mouse 1 (red line in Fig. 3f), which had little change in the tumor size, the V_{PD} value also did not change significantly. On the other hand, for the other mice with rapid increases in tumor size over time, the V_{PD} values increased proportionally to the changes in tumor size. Therefore, it was confirmed that cancer progression can be effectively monitored through our tumor growth monitoring system. However, the position of the device in the body may vary slightly due to the long-term movement of the mouse, resulting in a slight difference in the slope of the graph for each mouse, even with the device sutured in place. More accurate results can be obtained by using a larger animal model than a BALB/c nude mouse as an *in vivo* model and securely fixing the device in the body.

PDT with hyperthermia efficacy of system in vivo

To assess the efficacy of the system *in vivo* for photodynamic therapy (PDT) with hyperthermia, 5-ALA was injected intraperitoneally into the mice, and the μ -LED was wirelessly turned on at 100% intensity using a smartphone for 30 min after 4 h. The cancer therapy using our system was performed once a week for a total of three weeks (Fig. 4a). To further analyze the cancer therapeutic efficacy of the devices, groups treated with 5-ALA alone (5-ALA), device alone without μ -LED lighting (Device (-)), or devices alone with μ -LED lighting (Device (+)) were added to the analysis. The control group (Cont) did not receive any treatment for the tumor xenograft mice.

The tumor volume change rate for each group was measured by assessing the tumor volume at intervals of 3 to 4 days from the first treatment day for a total of 17 days (Fig. 4b). After 17 days of the first treatment, the tumor volume was found to be largest in the Cont group, followed by the Device (-), 5-ALA, Device (+) group, and significantly smaller in the 5-ALA/device (+) group compared to the Cont group ($p = 0.028$). As cancer progresses, tumors not only increase in volume but also induce weight loss due to disruption of the tight regulation of appetite and weight control by tumor-derived molecules³⁹. Indeed, the body weight of the Cont group decreased by 15.4% after 17 days compared to the first day of treatment, and the 5-ALA group and the Device (-) group decreased by 0.06% and 0.05%, respectively. In contrast, the body weight of the Device (+) group and the 5-ALA/device (+) group increased by 2.07% and 8.68%, respectively (Fig. 4c).

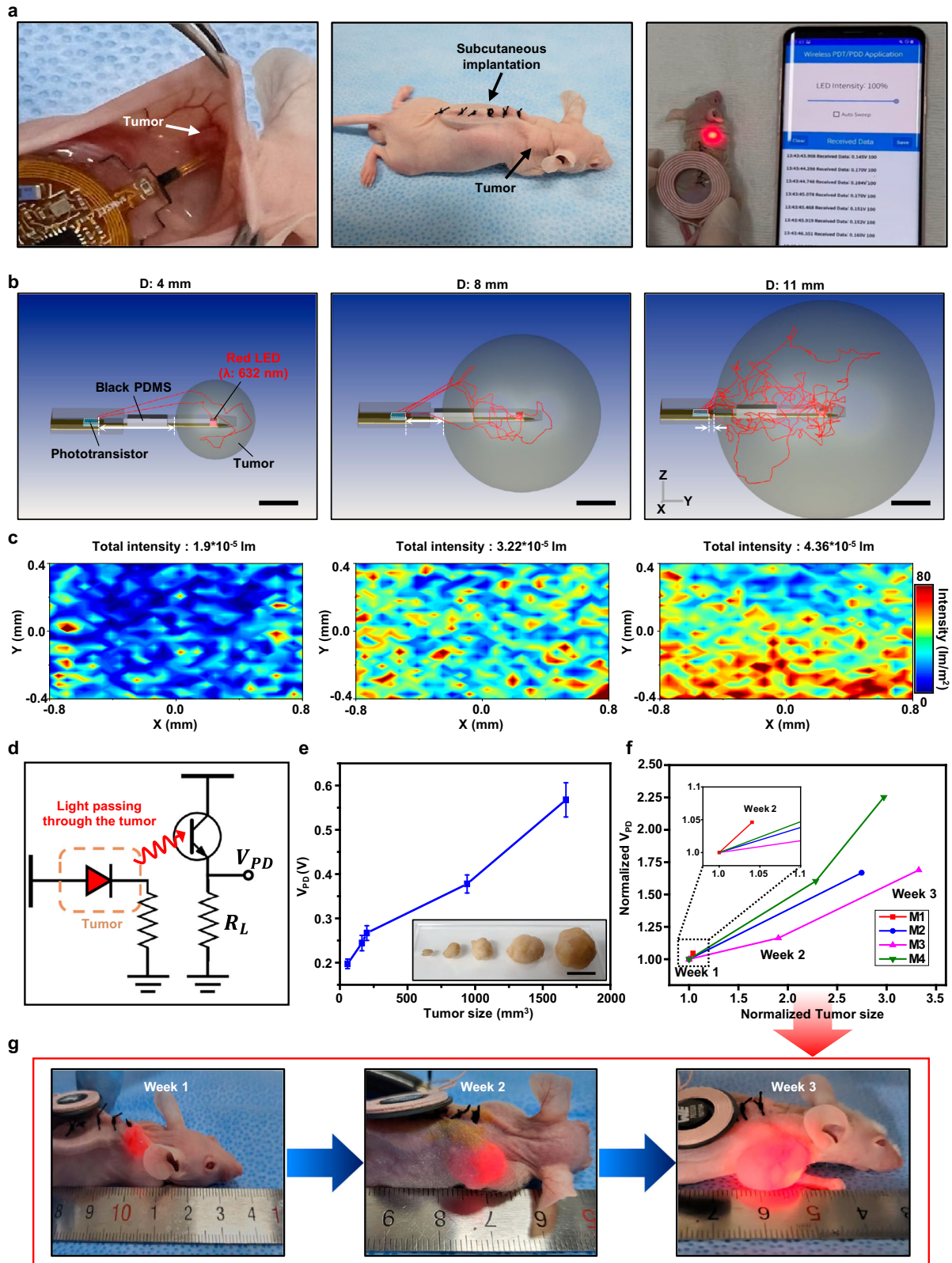
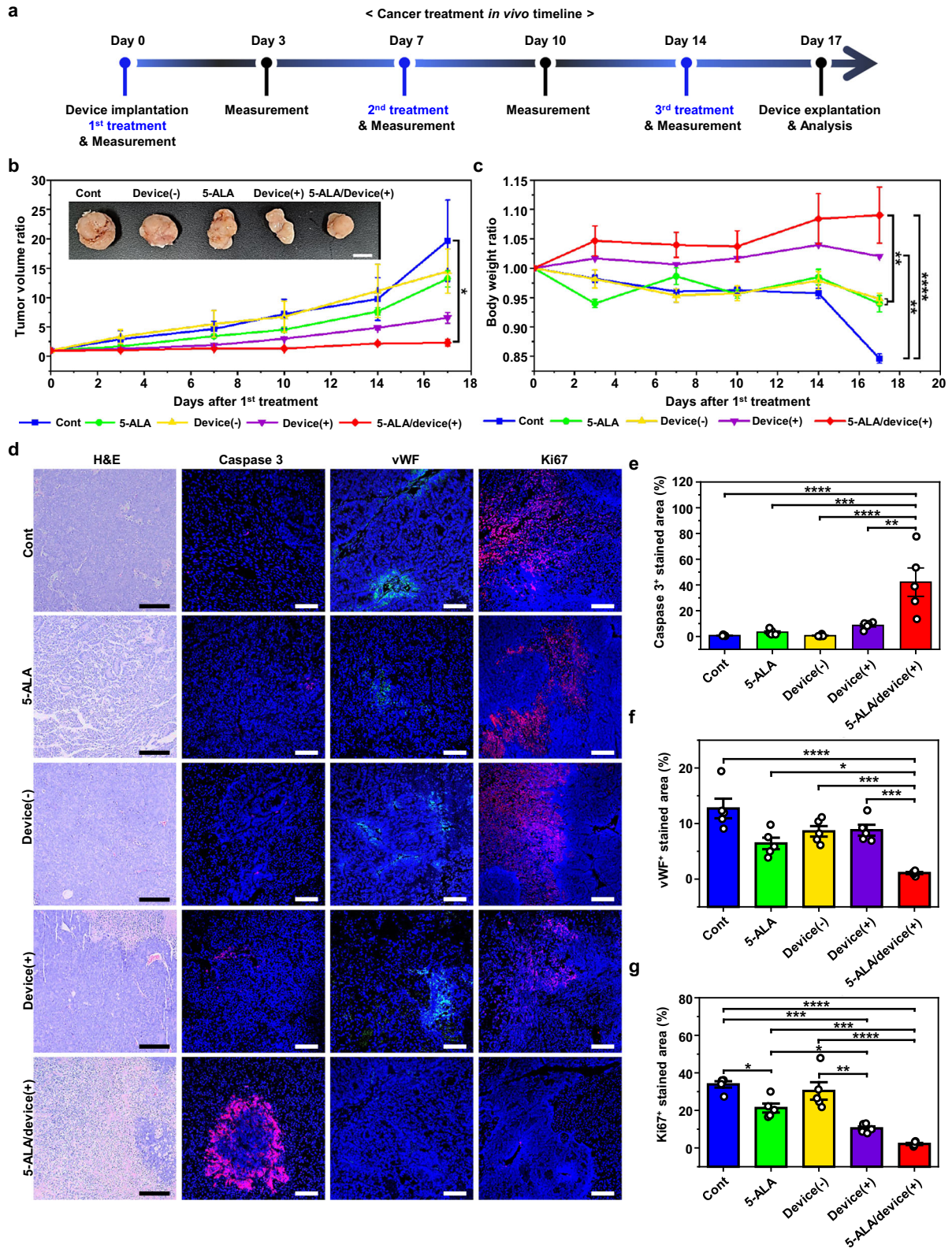


Fig. 3 Evaluation of tumor size monitoring system ex vivo and in vivo. **a** Pictures of the device's LED probe inserted into the tumor, the mouse model after device subcutaneously implanted, and wireless operation of the device after implantation. **b** Optical simulation results for the amount of light received by the phototransistor according to the size of the tumor. Scale bar, 2 mm. **c** The light distributions reaching each position inside the phototransistor derived from the optical simulation results. **d** Circuit diagram expressing how the device measures the amount of light in an in vivo environment. **e** Ex vivo experiments measuring phototransistor voltage (V_{PD}) values according to tumor size. Three devices with different insertion sites of tumors were exploited. Scale bar, 1 cm. **f** V_{PD} and tumor volume measured during the 3-week in vivo experiment. ($n = 4$). **g** Images of tumor size change in vivo over 3 weeks for M3.



We further analyzed tumor apoptosis, angiogenesis, and proliferation, which were promoted with tumor progression (Fig. 4d). H&E and caspase 3 immunofluorescent staining showed that in the 5-ALA/device (+) group, cellularity was significantly reduced, while the expression of caspase 3, which indicates apoptosis, effectively increased compared to all other groups in

the entire tumor region. Interestingly, in the case of the Device (+) group, almost no apoptosis was observed in the surface region of the tumor, but partial apoptosis was confirmed in the central region (Supplementary Fig. S10). These results are expected to be caused by the high heat generated from the μ -LED of the device when the light was turned on, suggesting the potential of the

Fig. 4 PDT with hyperthermia efficacy of system in vivo. **a** The timeline of in vivo experiments starting with device implantation on day 0 and performing cancer treatment and measurement until day 17. **b** The ratio of tumor volume at the indicated time points to initial tumor volume over time after first treatment for each group in human colorectal cancer cell (HCT-15)-based tumor xenograft mouse model ($n = 4$). Upper inset images are xenograft tumors excised from tumor xenograft mice treated with each treatment three times at one-week intervals. Scale bar, 1 cm. **c** The ratio of body weight at the indicated time points to initial body weight over time after first treatment for each group in human colorectal cancer cell (HCT-15)-based tumor xenograft mouse model ($n = 4$). **d** Histological and immunohistochemical evaluation of the excised xenograft tumors 3 weeks after first treatment. Hematoxylin and eosin (H&E) staining, and immunofluorescence staining for apoptosis (caspase 3, magenta region), angiogenesis (vWF, green region), cell proliferation (Ki67, magenta region). Nuclei were stained with DAPI (blue); scale bars, 200 μm for H&E, 50 μm for caspase 3, vWF and Ki67. **e–g** Cancer treatment efficacy of system as assessed by ratios of apoptosis (caspase 3), angiogenesis (vWF) and cell proliferation (Ki67) in the excised xenograft tumors 3 weeks after first treatment. Quantification of the **(e)** caspase 3-, **(f)** vWF-, and **(g)** Ki 67-positive fluorescence expression area (%) in the area of total cells ($n = 5$). Data are expressed as the mean \pm SEM. * $p < 0.05$, ** $p < 0.01$, *** $p < 0.001$, or **** $p < 0.0001$.

device as a hyperthermia treatment. Thermo-therapy applies heat 4 to 8 degrees higher than body temperature to the cancer site, and the device also increases in temperature by about 8 degrees at 100% light intensity²⁰. Conversely, in the 5-ALA group, apoptosis was partially observed in the surface region of the tumor, but little apoptosis was observed in the central region of the tumor. The apoptosis on the tumor surface of the 5-ALA group is expected to be due to the activation of PpIX, which accumulates in the tumor only on the surface exposed to daylight, consistent with the in vitro results. When the caspase 3+ stained area was quantified, the 5-ALA/device (+) group showed the highest expression ratio, followed by the Device (+) group, the 5-ALA group, and the Device (–) and Cont groups, which showed the lowest expression ratio (Fig. 4e).

5-ALA-based PDT is known for its ability to inhibit cancer cell proliferation and its anti-angiogenic effect^{40,41}. For these reasons, the effects of 5-ALA-based PDT using the device on tumor angiogenesis and cell proliferation were determined by immunofluorescence staining using von Willebrand factor (vWF) and Ki67 as vascular endothelial cell and cell proliferation markers, respectively. The proportion of vWF-positive areas was remarkably lower in the 5-ALA/device (+) group than in all other groups. In particular, there was no significant difference between the 5-ALA, Device (–), and Device (+) groups compared to the Cont group, but the vWF-positive area in the 5-ALA/device (+) group was reduced to 91.46% of the Cont group (Fig. 4f). The proportion of Ki67-positive areas was also the lowest in the 5-ALA/device (+) group at $2.11 \pm 0.56\%$, followed by the Device (+) group, the 5-ALA group, and the Device (–) group, and was the highest in the Cont group at $33.86 \pm 1.68\%$ (Fig. 4g). These results indicate that 5-ALA-based PDT using the device effectively inhibits angiogenesis and cancer cell proliferation.

Taken together, our system developed in this study not only maximizes the efficacy of 5-ALA-based PDT by enhancing apoptosis of cancer cells and effectively reducing angiogenesis and cell proliferation, but also shows potential as local hyperthermia through the heat generated by the μ -LED inserted into the tumor. Given these results, we confirmed the capability of the system to perform simultaneous monitoring of tumor size and treatment in a portable manner.

DISCUSSION

PDT combined with hyperthermia is a next-generation cancer treatment that can overcome the limitations of existing methods such as surgical ablation, chemotherapy, and radiation therapy. In this study, we developed a fully implantable and flexible optoelectronic device for unconventional PDT and demonstrated its potential as a powerful method to cure various cancers, including deeply located malignant tumors. The system we developed is fully implantable and operates wirelessly via wireless power transmission and BLE communications, allowing for seamless and tether-free measurements and treatments of tumors. Furthermore, the user can adjust the light intensity of

the μ -LED and monitor changes in tumor size using a smartphone application. In the future, it will be necessary to utilize low-intensity light and integrate a separate heater into the device to independently control the light and heat, and investigate the therapeutic effects of each. While this study was limited to measuring cancers located subcutaneously, our research holds significant value when external determination of tumor size is not feasible, and further research in this direction is planned. Overall, this study is expected to broaden the range of simultaneous cancer treatment and diagnosis options for patients by offering enhanced modalities.

METHODS

Fabrication of flexible and fully implantable wireless optoelectronic device

Flexible printed circuit boards composed of Cu/PI/Cu layers (18 $\mu\text{m}/25 \mu\text{m}/18 \mu\text{m}$) were custom-designed and fabricated by the manufacturer (ICBANQ). Circuit components, including a microcontroller (NRF52832, Nordic Semiconductor, Inc.), a μ -LED (APG0603SEC-E-T, Kingbright), a phototransistor (KDT00030, ON Semiconductor, Inc.), Schottky diodes (BAS40XY, Nexperia), a voltage regulator chip (LTC3255, Analog Devices, Inc.), crystal oscillators (KYOCERA AVX and Abracon), and other passive components such as resistors and capacitors, were manually soldered to the device using low-temperature solder paste (Sn42Bi58, KEK) (Supplementary Fig. S1 and Supplementary Table 1). The microcontroller (NRF52832) with Bluetooth Low Energy (BLE) was programmed in the Segger Embedded Studio using Embedded C language.

Encapsulation process for long-term in vivo experiment

First, the device was immersed in the adhesion promoter Silane A 174 (Sigma-Aldrich) and baked at 120 °C for 5 min. Then, a 4 μm -thick layer of Parylene-C was deposited using a parylene coating system (Femto Science). Subsequently, 50 nm of SiO₂ was deposited on the top and bottom of the device, respectively, using a sputtering system (LSP06, LAT). A Si wafer was deep cleaned using piranha solution (H₂SO₄:H₂O₂ = 3:1) at 100 °C for 15 min and surface-treated hydrophobically using a trichlorosilane solution (Sigma-Aldrich). PDMS (10:1 mixing ratio of base and curing agent) was spin-coated at 500 rpm on the Si wafer and cured at 120 °C for 30 min. After forming a chemical O–H group on the PDMS using O₂ plasma (Q190620-M01, Young Hi-Tech), the device was laminated and heated at 110 °C for 4 min to perform oxide bonding⁴². Then, the device was covered with a self-designed 3D-printed mold with a thickness of 0.5 mm, and PDMS (10:1 mixing ratio) was poured and cured under vacuum. The 3D-printed resin mold was removed from the wafer, and finally, PDMS (10:1 mixing ratio) mixed with edible black dye (10% wt to PDMS) was poured between the μ -LED and the phototransistor. After the black PDMS was completely cured, a self-standing device was obtained by manually cutting the PDMS on the bottom side along

the edge of the device and delaminating the device from the wafer. Supplementary Fig. S2 illustrates the schematics of the encapsulation process.

Smartphone application development for BLE communications and data processing

The Android smartphone application was developed in the Android Studio environment using the Kotlin programming language. The application connects to the BLE device by scanning for BLE advertising signals from the device and generating a BLE GATT (Generic Attribute Profile) connection after confirming the advertising signals. The data received from the BLE device is processed by reading the characteristic values of BLE GATT, and the processed data is saved in a text file and displayed in a real-time updated UI. To modulate the intensity of the μ -LED, UI-based programmable user inputs are encoded and transmitted to the BLE device by writing values to the BLE GATT characteristics.

Optical simulation for the light delivery in the device

3D ray-tracing simulations based on the Monte-Carlo method were carried out using commercial software (OpticStudio 16.0, ZEMAX, Inc.). In the simulation, a rectangular-shaped light source (0.80×0.35 mm in the x and y directions) with a wavelength of 632 nm was used. The light intensity of the source was 0.5 lumens (lm), and the background refractive index was 1.0. A rectangular detector (1.7×0.8 mm) with pixels of 30×30 in the x and y directions was used to capture the delivered light from the light source. The refractive indices of the PDMS and the PI substrate were 1.4 and 1.5, respectively. A Black PDMS model with a transmittance of $\sim 0.001\%$ was used based on the measurement results (see Supplementary Fig. 14). The optical constants for the human colon tumor appear in Supplementary Table 2. A total of 5×10^7 rays were used to obtain stable calculation results.

In vitro cytotoxicity of the device

For the evaluation of the cytotoxicity of the device, the viability of NIH-3T3 cells was analyzed in the extracted media according to ISO 10993-5:2009, as previously described⁴³. In brief, the extraction media were prepared as follows: the device, high-density polyethylene (negative), and ZDEC polyurethane (positive) samples were cut into 3 cm^2 and sterilized by soaking in 70% ethanol for one day and drying under a UV light for 4 h. Each sterilized sample was placed in fresh culture medium consisting of Dulbecco's modified eagle medium (Thermo Fisher Scientific, Waltham, MA, USA) supplemented with 10% fetal bovine serum (FBS; Thermo Fisher Scientific) and 1% penicillin-streptomycin (Thermo Fisher Scientific) and extracted for 72 h with shaking in a 37°C water bath. Then, each extraction medium was diluted at a 1:1 ratio of extraction medium to fresh culture medium. NIH-3T3 cells were seeded at a density of 1×10^4 cells per well in a flat-bottomed 96-well plate 24 h before being treated with each diluted extraction medium and incubated at 37°C for 24 h. Thereafter, the medium was removed and treated with a diluted cell counting kit-8 solution (Dojindo, Japan) for 4 h to analyze the cell viability. The absorbance of the reaction solution was measured at a wavelength of 490 nm using a 96-well plate reader (VersaMax; Molecular Devices, San Jose, CA, USA), and all samples were compared with a negative control to calculate the percentage of live cells.

Spectral characterization for PpIX

The absorbance spectrum of PpIX was characterized using an ultraviolet-visible-near-infrared spectrometer (Lambda 950, Perkin Elmer, Inc., USA) over the wavelength range of 450 to 700 nm. To avoid intramolecular interactions, PpIX powder (Sigma-Aldrich)

was diluted to 0.01 wt% in a Dimethyl Sulfoxide solution (Sigma-Aldrich).

Evaluation of in vitro PDT efficacy of device using HCT-15 cell-based tumor-mimic tissue

To prepare a human colorectal cancer cell-based tumor-mimicking tissue model, HCT-15 cells (ATCC, Manassas, VA, USA), a human colorectal cancer cell line, were embedded in a hydrogel solution composed of a 1:1 ratio of collagen type I (3 mg mL^{-1} ; CORNING, Corning, NY, USA) and fibrinogen (3 mg mL^{-1} ; Sigma-Aldrich, Saint Louis, MO, USA) at a concentration of 1×10^7 cells/mL. To fabricate a tumor-mimicking tissue model with a diameter of 3 cm and a height of 5 mm, 5 mL of hydrogel solution was added to a 6-well plate, and the pH was adjusted to 7.0 using 1 N sodium hydroxide (Sigma-Aldrich). 2 U mL^{-1} of thrombin (Sigma-Aldrich) was then added, followed by incubation at 37°C for 30 min to gel. The hydrogel containing HCT-15 cells was then immersed in HCT-15 cell medium consisting of Roswell Park Memorial Institute (RPMI) 1640 medium (Thermo Fisher Scientific) supplemented with 10% FBS (Thermo Fisher Scientific) and 1% penicillin-streptomycin (Thermo Fisher Scientific), and cultured at 37°C for 1 day to form a stabilized tumor-mimicking tissue model. The medium was then replaced with HCT-15 cell medium containing 1 mM 5-ALA (Sigma-Aldrich). After 3 h, the 5-ALA-containing medium was replaced with PBS, and the μ -LED of the device was inserted into the center of the tumor-mimicking tissue. The tumor-mimicking tissue was then irradiated with LED light using the μ -LED. After irradiation, the PBS was replaced with fresh HCT-15 cell medium immediately.

The in vitro study was conducted in two ways: to confirm the PDT efficacy of the device and to investigate PDT efficacy according to light intensities. Four groups were established to investigate PDT efficacy of the device: the control group, the 5-ALA group, the 5-ALA/device (−) group, and the 5-ALA/device (+) group. The control group did not receive any treatment on the tumor-mimic tissue, and the 5-ALA group was treated with only 5-ALA. The 5-ALA/device (−) group treated the tumor-mimic tissue with 5-ALA and applied the device but did not irradiate the LED light. The 5-ALA/device (+) group received LED light irradiation at 5 mW through the μ -LED of the applied device after 5-ALA was treated on the tumor-mimic tissue. After each group was treated in this way for 1 day, the cell viability of the tumor-mimic tissues was evaluated using the LIVE/DEAD assay (LIVE/DEAD™ Viability/Cytotoxicity Kit; Thermo Fisher Scientific)⁴⁴. Briefly, the tumor-mimic tissues were washed in phosphate-buffered saline (PBS; Thermo Fisher Scientific) and then treated with a solution containing $5 \mu\text{L}$ calcein-AM and $20 \mu\text{L}$ ethidium homodimer-1 in 10 mL PBS. The tumor-mimic tissues were then incubated at 37°C for 20 min and immediately imaged using a laser scanning confocal microscope (LSM 700; Carl Zeiss, Oberkochen, Germany). Cell viability was quantified using Image J software in regions 0, 7, and 15 mm away from the center of the tumor-mimic tissues, respectively ($n = 3$).

To evaluate PDT efficacy according to light intensities, the device was applied to the tumor-mimic tissues treated with 5-ALA, and LED lights of 0, 30, 70, and 100% of maximum brightness were respectively irradiated through the μ -LED. After that, cell viability was evaluated in the same manner as before at a distance of 0, 5, 10, and 15 mm from the μ -LED inserted into the tumor-mimic tissues ($n = 4$).

In vivo PDT with hyperthermia and tumor size measurement with devices using HCT-15 cell-based tumor xenograft mouse model

All animal maintenance and in vivo experiments were conducted in accordance with the regulations of the Institutional Animal Care and Use Committee of the Korea Institute of Science and

Technology (study approval number: KIST-2021-08-095). To establish the HCT-15 cell-based tumor xenograft mouse model, 1×10^7 HCT-15 cells suspended in 200 μL of PBS were subcutaneously injected into the dorsal flanks of 7-week-old BALB/c nude mice (NARA bio, South Korea). After 2 weeks, the experiment was initiated when the longest diameter of the tumor reached 5–7 mm. To evaluate the in vivo PDT efficacy of the device, tumor xenograft mice were first injected intraperitoneally with 250 mg kg⁻¹ of 5-ALA. Four hours later, the tumor xenograft mice were anesthetized with isoflurane, and an approximately 2 cm incision was made on the dorsal skin around the tumor of each mouse for implantation of the device. The device was then implanted subcutaneously, and the $\mu\text{-LED}$ part was inserted into the tumor. After suturing the incised dorsal skin, a coil (resonant frequency: 13.56 MHz \pm 40 kHz) connected to a function generator (Tektronix; 10 V, 13.56 MHz) was placed over the skin near the implanted device to turn on the light of $\mu\text{-LED}$ inserted into the tumor, and the $\mu\text{-LED}$ light was irradiated inside the tumor for 30 min. PDT using the device was repeated once a week. The individual tumor volume and body weights of mice were observed for 17 days at 3-day intervals from the first day of treatment. Tumor volume was calculated using the following formula based on the length and width values of the tumor measured with calipers⁴⁵: Tumor volume = (width² \times length) / 2. Three days after the last treatment, mice were sacrificed and tumors were explanted. The explanted tumors were fixed in 4% paraformaldehyde (BIOSESANG, Seoul, South Korea) for 1 day, then embedded in paraffin, and sectioned at a thickness of 6 μm using a microtome (RM2255; Leica, Wetzlar, Germany) for histological analysis.

In vivo biocompatibility of the device

The devices were implanted subcutaneously under the dorsal skin of 7-week-old Sprague-Dawley rats (SD rats; NARA bio). The implanted devices were explanted, along with the surrounding tissues, 5 and 14 days after surgery to confirm acute and chronic inflammatory responses. The explanted devices and surrounding tissues were fixed in 4% paraformaldehyde for 1 day, and the devices were carefully removed to avoid damaging the surrounding tissue. Subsequently, the tissues were embedded in paraffin and sectioned at a thickness of 6 μm using a microtome for histological analysis.

H&E and MT staining

H&E staining was carried out by following standard protocols. Briefly, deparaffinized tissue sections were first stained with hematoxylin solution (Abcam, Cambridge, UK) for 13 min. After extensive washing with running tap water and 80% alcohol, the slides were stained with eosin Y solution for 6 min. For MT staining, the deparaffinized tissue sections were first stained with hematoxylin solution (Abcam) for 13 min and then washed with running tap water for 5 min. The sections were then stained with biebrich scarlet-acid fuchsin solution (Sigma-Aldrich) for 5 minutes and rinsed with distilled water. Subsequently, the phosphomolybdic/phosphotungstic acid solution (Sigma-Aldrich) was treated for 10 min, discarded, and immediately treated with methyl blue solution (Sigma-Aldrich) for 1 min to stain the sections. All stained sections were observed under a light microscope (ECLIPSE Ts2R; Nikon, Tokyo, Japan).

Immunofluorescence staining

For immunofluorescence staining, tissue sections were deparaffinized, blocked with 4% bovine serum albumin (BSA), and then incubated with primary antibodies or primary antibodies conjugated with fluorescence dyes. In the case of the primary antibodies to which the fluorescent dyes were not conjugated, the corresponding secondary antibodies were treated after the primary

antibodies treatment. Anti-cluster of differentiation 68 (CD68) conjugated with Alexa Fluor 594 (1:50; Santa Cruz Biotechnology, Dallas, TX, USA) and anti-CD206 conjugated with Alexa Fluor 488 (1:50; Santa Cruz Biotechnology) were used to estimate the immune response by M1 and M2 macrophages, respectively. Apoptosis in tumor tissues was confirmed by anti-caspase 3 conjugated with Alexa Fluor 594 (1:50; Santa Cruz Biotechnology). Angiogenesis of tumor tissue was confirmed by rabbit polyclonal anti-von Willebrand factor (vWF at 1:100; Abcam) as a primary antibody and anti-rabbit IgG conjugated with Alexa fluor 488 (1:500; Invitrogen) as a secondary antibody. Tumor cell proliferation was confirmed by mouse monoclonal anti-Ki 67 (1:100; Abcam) as primary antibody and anti-mouse IgG conjugated with Alexa fluor 594 (1:500; Invitrogen) as secondary antibody.

Statistical analysis

All data are presented as the mean \pm standard error of the mean (SEM) and were analyzed by one-way analysis of variance (ANOVA) with Tukey's significant difference post hoc test. A p - values less than 0.05 were considered statistically significant. Statistical analyses were performed using Origin 2022 software (OriginLab Corporation).

DATA AVAILABILITY

The data that support the findings of this study are available from the corresponding author upon reasonable request.

CODE AVAILABILITY

The code that support the figures of this study is available from the corresponding author upon reasonable request.

Received: 23 May 2023; Accepted: 16 August 2023;

Published online: 28 August 2023

REFERENCES

1. Ferlay, J. et al. Cancer statistics for the year 2020: an overview. *Int. J. Cancer* **149**, 778–789 (2021).
2. Bentzen, S. M. Preventing or reducing late side effects of radiation therapy: radiobiology meets molecular pathology. *Nat. Rev. Cancer* **6**, 702–713 (2006).
3. Carelle, N. et al. Changing patient perceptions of the side effects of cancer chemotherapy. *Cancer* **95**, 155–163 (2002).
4. Ciesielski, M. et al. Analysis of postoperative morbidity and mortality following surgery for gastric cancer. Surgeon volume as the most significant prognostic factor. *Prz. Gastroenterol.* **12**, 215–221 (2017).
5. Lange, M. M. & Van De Velde, C. J. Urinary and sexual dysfunction after rectal cancer treatment. *Nat. Rev. Urol.* **8**, 51–57 (2011).
6. Schmitz, K. H., Speck, R. M., Rye, S. A., DiSipio, T. & Hayes, S. C. Prevalence of breast cancer treatment sequelae over 6 years of follow-up: the pulling through study. *Cancer* **118**, 2217–2225 (2012).
7. Bray, F. N., Simmons, B. J., Wolfson, A. H. & Nouri, K. Acute and chronic cutaneous reactions to ionizing radiation therapy. *Dermatol. Ther. (Heidelb.)* **6**, 185–206 (2016).
8. Wang, K. & Tepper, J. E. Radiation therapy-associated toxicity: etiology, management, and prevention. *CA Cancer J. Clin.* **71**, 437–454 (2021).
9. Tao, J. J., Visvanathan, K. & Wolff, A. C. Long term side effects of adjuvant chemotherapy in patients with early breast cancer. *Breast* **24**, S149–S153 (2015).
10. Azim Jr, H., De Azambuja, E., Colozza, M., Bines, J. & Piccart, M. Long-term toxic effects of adjuvant chemotherapy in breast cancer. *Ann. Oncol.* **22**, 1939–1947 (2011).
11. Schagen, S. B., Tsvetkov, A. S., Compter, A. & Wefel, J. S. Cognitive adverse effects of chemotherapy and immunotherapy: are interventions within reach? *Nat. Rev. Neurol.* **18**, 173–185 (2022).
12. Sun, B., Rahmat, J. N. B. & Zhang, Y. Advanced techniques for performing photodynamic therapy in deep-seated tissues. *Biomaterials* **291**, 121875 (2022).
13. Agostinis, P. et al. Photodynamic therapy of cancer: an update. *CA Cancer J. Clin.* **61**, 250–281 (2011).
14. Bansal, A., Yang, F., Xi, T., Zhang, Y. & Ho, J. S. In vivo wireless photonic photodynamic therapy. *PNAS* **115**, 1469–1474 (2018).
15. Chilakamarthi, U. & Giribabu, L. Photodynamic therapy: past, present and future. *Chem. Rec.* **17**, 775–802 (2017).

16. Kim, M. M. & Darafsheh, A. Light sources and dosimetry techniques for photodynamic therapy. *Photochem. Photobiol.* **96**, 280–294 (2020).
17. Yamagishi, K. et al. Tissue-adhesive wirelessly powered optoelectronic device for metronomic photodynamic cancer therapy. *Nat. Biomed. Eng.* **3**, 27–36 (2019).
18. Kim, W. S. et al. Al-enabled, implantable, multichannel wireless telemetry for photodynamic therapy. *Nat. Commun.* **13**, 2178 (2022).
19. Choi, J. et al. Implantable micro-scale LED device guided photodynamic therapy to potentiate antitumor immunity with mild visible light. *Biomater. Res.* **26**, 1–15 (2022).
20. Engelmann, U. M. et al. Combining bulk temperature and nanoheating enables advanced magnetic fluid hyperthermia efficacy on pancreatic tumor cells. *Sci. Rep.* **8**, 13210 (2018).
21. Chu, K. F. & Dupuy, D. E. Thermal ablation of tumours: biological mechanisms and advances in therapy. *Nat. Rev. Cancer* **14**, 199–208 (2014).
22. Zhu, L. et al. Ultrasound hyperthermia technology for radiosensitization. *Ultrasound Med Biol.* **45**, 1025–1043 (2019).
23. Johannsen, M., Thiesen, B., Wust, P. & Jordan, A. Magnetic nanoparticle hyperthermia for prostate cancer. *Int. J. Hyperth.* **26**, 790–795 (2010).
24. Zhang, W. et al. Real-time, volumetric imaging of radiation dose delivery deep into the liver during cancer treatment. *Nat. Biotechnol.* **41**, 1160–1167 (2023).
25. Prasad, S. R. et al. CT tumor measurement for therapeutic response assessment: comparison of unidimensional, bidimensional, and volumetric techniques—initial observations. *Radiology* **225**, 416–419 (2002).
26. Abramson, A. et al. A flexible electronic strain sensor for the real-time monitoring of tumor regression. *Sci. Adv.* **8**, eabn6550 (2022).
27. Miao, J. et al. Heavy atom-free, mitochondria-targeted, and activatable photosensitizers for photodynamic therapy with real-time in-situ therapeutic monitoring. *Angew. Chem., Int. Ed. Engl.* **61**, e202201815 (2022).
28. Gao, Y. et al. A dual-functional photosensitizer for ultraefficient photodynamic therapy and synchronous anticancer efficacy monitoring. *Adv. Funct. Mater.* **29**, 1902673 (2019).
29. Yu, Q. et al. Reductant-free synthesis of MnO₂ nanosheet-decorated hybrid nanoplatform for magnetic resonance imaging-monitored tumor microenvironment-responsive chemodynamic therapy and near-infrared-mediated photodynamic therapy. *Small Struct.* **2**, 2100116 (2021).
30. Ma, H. et al. A versatile theranostic nanoplatform with aggregation-induced emission properties: fluorescence monitoring, cellular organelle targeting, and image-guided photodynamic therapy. *Small* **19**, 2204778 (2023).
31. Huang, K. et al. EGFR-targeted photosensitizer for enhanced photodynamic therapy and imaging therapeutic effect by monitoring GSH decline. *Sens. Actuators B Chem.* **355**, 131275 (2022).
32. Zhang, L. et al. Computed tomography and photoacoustic imaging guided photodynamic therapy against breast cancer based on mesoporous platinum with insitu oxygen generation ability. *Acta Pharm. Sin. B.* **10**, 1719–1729 (2020).
33. Chiang, C.-H. et al. Development of a neural interface for high-definition, long-term recording in rodents and nonhuman primates. *Sci. Transl. Med.* **12**, eaay4682 (2020).
34. Song, K.-I. et al. Adaptive self-healing electronic epineurium for chronic bidirectional neural interfaces. *Nat. Commun.* **11**, 4195 (2020).
35. Kang, K., Cho, Y. & Yu, K. J. Novel nano-materials and nano-fabrication techniques for flexible electronic systems. *Micromachines* **9**, 263 (2018).
36. Henderson, B. W., Busch, T. M. & Snyder, J. W. Fluence rate as a modulator of PDT mechanisms. *Lasers Surg. Med.* **38**, 489–493 (2006).
37. Kim, M. P. et al. Generation of orthotopic and heterotopic human pancreatic cancer xenografts in immunodeficient mice. *Nat. Protoc.* **4**, 1670–1680 (2009).
38. Carvalho, S. et al. in *Dynamics and Fluctuations in Biomedical Photonics XIV*. 218–233 (SPIE).
39. Johnen, H. et al. Tumor-induced anorexia and weight loss are mediated by the TGF- β superfamily cytokine MIC-1. *Nat. Med.* **13**, 1333–1340 (2007).
40. Nakayama, T. et al. Dormant cancer cells accumulate high protoporphyrin IX levels and are sensitive to 5-aminolevulinic acid-based photodynamic therapy. *Sci. Rep.* **6**, 1–12 (2016).
41. Kawczyk-Krupka, A. et al. Secretion of the angiogenic factor VEGF after photodynamic therapy with ALA under hypoxia-like conditions in colon cancer cells. *Photodiagnosis Photodyn. Ther.* **21**, 16–18 (2018).
42. Lee, J. Y. et al. Foldable three dimensional neural electrode arrays for simultaneous brain interfacing of cortical surface and intracortical multilayers. *npj Flex Electron* **6**, 86 (2022).
43. Park, T. H. et al. Highly sensitive on-skin temperature sensors based on biocompatible hydrogels with thermoresponsive transparency and resistivity. *Adv. Healthc. Mater.* **10**, 2100469 (2021).
44. Yoo, J. et al. Use of elastic, porous, and ultrathin co-culture membranes to control the endothelial barrier function via cell alignment. *Adv. Funct. Mater.* **31**, 2008172 (2021).
45. Lee, H. et al. Combinatorial inhibition of cell surface receptors using dual aptamer-functionalized nanoconstructs for cancer treatment. *Pharmaceutics* **12**, 689 (2020).

ACKNOWLEDGEMENTS

This work acknowledges the support received from the National Research Foundation of Korea (Grant Nos. NRF-2019R1A2C2086085, 2023R1A2C3004531) and the Korean Fund for Regenerative Medicine (KFRM) grant funded by the Korea government (the Ministry of Science and ICT, the Ministry of Health & Welfare) (21A0504L1–11). Images in Fig. 1a from 3D Rat Anatomy Software (www.biosphera.org).

AUTHOR CONTRIBUTIONS

Y.M.S., Y.J. and K.J.Y. jointly supervised this work. K.K., I.S.M. and T.H.K. have contributed equally to this work. K.K., I.S.M. and T.H.K. designed research. K.K., I.S.M., S.H., K.K. and K.K. fabricated device. D.H.K. performed ray-tracing simulation. K.K., I.S.M. and T.H.K. performed the in vitro experiments. K.K., I.S.M., T.H.K., S.P., J.L. performed the in vivo experiments. T.H.K., S.P. and J.L. performed cell viability and biocompatibility test. T.H.K., S.P. and J.L. performed histology. I.S.M. programmed BLE firmware and smartphone application. K.K., I.S.M. and T.H.K. performed data analysis. K.K., I.S.M., T.H.K., D.H.K., Y.M.S., Y.J. and K.J.Y. wrote the manuscript.

COMPETING INTERESTS

The authors declare no competing interests.

ADDITIONAL INFORMATION

Supplementary information The online version contains supplementary material available at <https://doi.org/10.1038/s41528-023-00276-x>.

Correspondence and requests for materials should be addressed to Young Min Song, Youngmee Jung or Ki Jun Yu.

Reprints and permission information is available at <http://www.nature.com/reprints>

Publisher's note Springer Nature remains neutral with regard to jurisdictional claims in published maps and institutional affiliations.



Open Access This article is licensed under a Creative Commons Attribution 4.0 International License, which permits use, sharing, adaptation, distribution and reproduction in any medium or format, as long as you give appropriate credit to the original author(s) and the source, provide a link to the Creative Commons license, and indicate if changes were made. The images or other third party material in this article are included in the article's Creative Commons license, unless indicated otherwise in a credit line to the material. If material is not included in the article's Creative Commons license and your intended use is not permitted by statutory regulation or exceeds the permitted use, you will need to obtain permission directly from the copyright holder. To view a copy of this license, visit <http://creativecommons.org/licenses/by/4.0/>.

© The Author(s) 2023